catalysts

MDPI

Article

Promotion Effects of Ce-Doping on Catalytic Oxidation of Ethane over $Pt/Ce_xTi_{1-x}O_2$

Dengmao Wu [1,2], Xianyan Lv [1,2], Xiurong Ren [3], Changming Hou [1,2], Qianwei Ma [4], Junxuan Yao [1,2,*] and Jiangliang Hu [1,2,5,*]

1 State Key Laboratory of Clean and Efficient Coal Utilization, Taiyuan University of Technology, Taiyuan 030024, China; wudengmao0888@link.tyut.edu.cn (D.W.); lvxianyan1998@163.com (X.L.); houchangming1010@link.tyut.edu.cn (C.H.)
2 College of Chemical Engineering and Technology, Taiyuan University of Technology, Taiyuan 030024, China
3 College of Mechanical and Vehicle Engineering, Taiyuan University of Technology, Taiyuan 030024, China; renxiurong@tyut.edu.cn
4 College of Civil Engineering, Taiyuan University of Technology, Taiyuan 030024, China; maqw2019@163.com
5 Shanxi Zhejiang University New Materials and Chemical Research Institute, Taiyuan 030024, China
* Correspondence: yaojunxuan@sxri.hrl.ac.cn (J.Y.); hujiangliang@tyut.edu.cn (J.H.)

Abstract: The catalytic oxidation of VOCs is widely acknowledged as the most available technology to reduce air pollution. Among the catalysts for VOCs, 1 wt%-Pt/TiO_2 catalysts using metal as a doping element have shown amazing potential in many fields. However, achieving high catalytic performance at relatively low temperatures based on the activation of molecules is still a formidable challenge owing to the catalytic activity being highly dependent on temperature. Here, the role of the rare earth metal Ce in the catalytic oxidation of ethane was studied by preparing $Pt/Ce_xTi_{1-x}O_2$ (x = 0, 0.002, 0.005, 0.01, 0.02, and 0.05) catalysts. When the Ce/(Ce+Ti) molar ratio was 0.01, $Pt/Ce_{0.01}Ti_{0.99}O_2$ achieved 90% ethane conversion at 436 °C. This reaction temperature is 15% lower than that for Pt/TiO_2. The characterization results show that the doping of Ce caused lattice expansion of TiO_2 and its distortion brought about by oxygen vacancies. Additionally, the appropriate amount of Ce-doping can alter the interaction between the active component Pt and the carrier TiO_2, thereby improving the activity and concentration of the active surface lattice oxygen species of the catalyst. These results provide a foundation for the design of the catalytic oxidation of VOCs under mild operating conditions.

Keywords: VOCs; Pt-based catalyst; catalyst carrier; catalysis; oxidation; Ce-doping

Citation: Wu, D.; Lv, X.; Ren, X.; Hou, C.; Ma, Q.; Yao, J.; Hu, J. Promotion Effects of Ce-Doping on Catalytic Oxidation of Ethane over $Pt/Ce_xTi_{1-x}O_2$. *Catalysts* **2023**, *13*, 626. https://doi.org/10.3390/catal13030626

Academic Editor: Giuseppe Pantaleo

Received: 22 January 2023
Revised: 2 March 2023
Accepted: 2 March 2023
Published: 21 March 2023

1. Introduction

Volatile organic compounds (VOCs) are a class of numerous gas pollutants including hydrocarbons (alkanes, olefins, and aromatics), ketones, esters, alcohols, etc. Produced by industrial sources, VOCs are discharged into the atmosphere, leading to photochemical reactions when encountering other pollutants, such as nitrogen oxides (NO_x) and sulfur dioxide (SO_2), under certain conditions. This generates fine particles, ozone, and other secondary pollutants [1,2]. Ethane is a significant low-weight VOC that results from the gasification of coal, the outgassing of rock oil, and a variety of chemical reactions. Compared with other VOCs, ethane is more difficult to be totally oxidized [3]. These products can aggravate urban haze pollution, damage human organs and the nervous system, and increase the likelihood of cancer in citizens [4,5]. Therefore, it is important to reduce the number of discharged VOCs, especially ethane. The catalytic oxidation of VOCs has been recognized as the most promising technology, and several studies have been conducted to increase its reaction rate. Jian et al. [6] reported that solvothermally prepared nanosphere α-Fe_2O_3 exhibited satisfactory ethane catalytic combustion activity and stability that greatly improved the concentration of reactive oxygen species, the oxygen

transfer rate, and the redox properties of the catalyst due to more oxygen vacancies and lattice defects. In addition, DFT results showed that the oxygen vacancy formation energy of nanosphere α-Fe_2O_3 was the lowest and that the adsorption energy of ethane and O_2 was the strongest, which could accelerate the ethane oxidation process. Guo et al. [7] introduced different amounts of Fe, Bi, and Ce to change the performance of manganese-based oxide catalysts. MnO_x(MS)-5%Fe, MnO_x(MS)-15%Bi, and MnO_x(MS)-10%Ce catalysts were observed to significantly change the catalytic performance in removing oxygen-containing VOCs because of a larger specific surface area, higher active surface oxygen, higher Mn ion concentration, and better reducibility at low temperatures. Consequently, increasing surface defect sites and the active surface oxygen concentration by doping is a common method for catalyst modification.

However, due to the lack of active sites with strong oxidation ability, non-noble-metal oxides with poor oxidation activity cannot meet the requirements of practical industrial applications and thus are used as carriers in many cases. Therefore, highly active noble-metal catalysts are more widely used in VOC catalytic oxidation applications. Yu et al. [8] reported that the oxygen vacancy-rich Ru/TiO_2 catalyst exhibited excellent activity and stability in the oxidation of mixed VOCs, which could inhibit the production of by-products and Cl_2. At present, Pt-based catalysts play an increasingly important role in the catalytic removal of VOCs. By manipulating the chemical properties of the multi-component interface, Mi Yoo [9] synthesized dense Pt single atoms that were shown to be highly reactive to oxidation reactions and optimized the catalytic performance of noble-metal single-atom catalysts by means of the atomic-scale tuning of the metal support interface. Ye [10] prepared hierarchical Pt/Co_3O_4-NiO catalysts that showed a hollow porous structure with characteristics of low air resistance, fast diffusion channels, and abundant active oxygens at the interface between Co_3O_4 and NiO. Oxygen vacancies generated during Pt deposition were favorable to the adsorption and conversion of HCHO, and the electron transfer from NiO to Pt enhanced the adsorption and activation of O_2. Due to the advantages described above, the novel catalyst presented excellent activity. In Pt-based catalyst systems, other metal elements are often introduced to increase the interaction between the catalyst active component and the support. The doping of rare earth elements, e.g., La [11], Ce, etc., can improve catalytic activity; furthermore, Ce has good oxygen storage performance. Chen et al. [12] reported a study in which Pt was supported using CeO_2-Al_2O_3. Due to the strong interaction between Pt and CeO_2, it showed high stability and catalytic activity in the catalytic oxidation of dichloromethane. H_2-TPR, NH_3-TPD, and other characterization results demonstrated that the optimal combination of surface acidity and redox properties of the catalyst synergistically contributed to its high activity. The interaction between the noble metal and the support also improved the oxygen mobility of CeO_2 and accelerated the oxidation of Cl_2 by Cl ions.

Under this condition, Ce was introduced into a Pt/TiO_2 system to construct a CeO_2-TiO_2 composite carrier in many recent studies [13–15]. However, few reports focused on the change in oxygen vacancies and oxygen species caused by the change in the carrier lattice structure owing to the introduction of Ce. In this study, Ce was utilized as a doping modifier for the amendment of structural defects on the surface of the Pt/TiO_2 catalyst with an in situ doping method to increase oxygen vacancies and the active surface lattice oxygen concentration and promote the interaction among the Pt active component, the Ce-doping element, and the TiO_2 carrier. The catalytic performance of 1 wt%-$Pt/Ce_xTi_{1-x}O_2$ catalysts with different Ce/Ti molar ratios was compared using ethane as a typical reactant. The results suggest that $Pt/Ce_xTi_{1-x}O_2$ catalysts can improve the deep oxidation activity of ethane and that the temperature of T_{90} of the $Pt/Ce_{0.01}Ti_{0.99}O_2$ catalyst can be as low as 436 °C. XRD, N_2 adsorption–desorption, SEM, XPS, H_2-TPR, O_2-TPD, and NH_3-TPD were carried out to characterize the physicochemical properties of the catalysts and indicate the relationship between structure and catalyst activity. In addition, the resistance ability of the catalysts to sulfur and water was also measured.

2. Results and Discussion

2.1. Catalytic Activity

2.1.1. Catalytic Performance in Ethane Oxidation

In the preliminary preparations, we prepared Pt/M-TiO_2 catalysts (M = Ce, Mg, Ni, Mn, Co, Sn, Ca, La, W, V, Zr, Mo, Sm, Fe, Cr, and Cu; M:Ti (molar ratio) was fixed at 1:99), which were used to evaluate the activity and durability of catalysts in a complex atmosphere. Figure 1a,b present the ethane conversion rates of these catalysts at different temperatures and over time, respectively. It can be seen that the Pt/$Ce_{0.01}Ti_{0.99}O_2$ catalyst showed the best catalytic oxidation activity and stability; therefore, Ce was selected as the doping modification additive for this study. Figure 1c and Figure S1 show the activity evaluation curves of Pt/$Ce_xTi_{1-x}O_2$ (x = 0, 0.002, 0.005, 0.01, 0.02, and 0.05) catalysts and the corresponding supports, i.e., $Ce_{0.01}Ti_{0.99}O_2$ and TiO_2, where TiO_2 was observed to have nearly no catalytic oxidation ability for ethane. Apparently, the catalytic ability of $Ce_{0.01}Ti_{0.99}O_2$ is limited when doping Ce, indicating that it is not an active component. After loading Pt, however, the activity of Pt/TiO_2 was greatly improved due to the strong catalytic oxidation performance of Pt and the possible interaction among metal elements. The catalytic activity of the Pt/$Ce_xTi_{1-x}O_2$ (x = 0.002, 0.005, 0.01, 0.02, and 0.05) catalysts was improved to varying degrees compared with that of the Pt/TiO_2 catalysts without doping the Ce element due to a possible interaction among the metal elements. In addition, the activity first increased but then decreased with the increase in the proportion of the Ce element, and the catalyst doped with 1% Ce exhibited the best ethane catalytic oxidation activity (T_{90} = 436 °C). The diminishing order of catalytic activity at 90% ethane conversion was as follows: Pt/$Ce_{0.01}Ti_{0.99}O_2$, Pt/$Ce_{0.005}Ti_{0.995}O_2$, Pt/$Ce_{0.02}Ti_{0.98}O_2$, Pt/$Ce_{0.05}Ti_{0.95}O_2$, and Pt/$Ce_{0.002}Ti_{0.998}O_2$ (see Table 1), and this shows that excessive or insufficient doping is detrimental to the improvement of catalyst activity. Figure 1d describes the Arrhenius plots of the Pt/$Ce_xTi_{1-x}O_2$ (x = 0, 0.002, 0.005, 0.01, 0.02, and 0.05) catalysts. The trend of apparent activation energy was opposite to the that of the T_{90} data, and Pt/$Ce_{0.01}Ti_{0.99}O_2$ had the lowest apparent activation energy, indicating that the reactant molecules in the catalytic oxidation of ethane were more easily activated on the catalyst and that the catalytic oxidation performance was the best.

Table 1. Catalytic activity and Ea values of Pt/$Ce_xTi_{1-x}O_2$ (x = 0, 0.002, 0.005, 0.01, 0.02, and 0.05) catalysts.

Catalyst	T_{50} [1] (°C)	T_{90} [1] (°C)	Ea (kJ/mol)	T_{50} [2] (°C)	T_{90} [2] (°C)
Pt/TiO_2	441	514	79.54	345	413
Pt/$Ce_{0.02}Ti_{0.98}O_2$	439	500	72.31	348	441
Pt/$Ce_{0.05}Ti_{0.95}O_2$	390	455	57.92	321	416
Pt/$Ce_{0.01}Ti_{0.99}O_2$	360	436	48.84	316	370
Pt/$Ce_{0.02}Ti_{0.98}O_2$	389	460	62.82	326	472
Pt/$Ce_{0.05}Ti_{0.95}O_2$	407	466	70.75	403	490

[1] Temperature at which conversion was 50% or 90%. Reaction conditions: [C_2H_6] = 1000 ppm, [O_2] = 4 vol%, and balance N_2. [2] Temperature at which conversion was 50% or 90%. Reaction conditions: [C_2H_6] = 1000 ppm, [O_2] = 4 vol%, [H_2O] = 5%, [SO_2] = 100 ppm, and balance N_2.

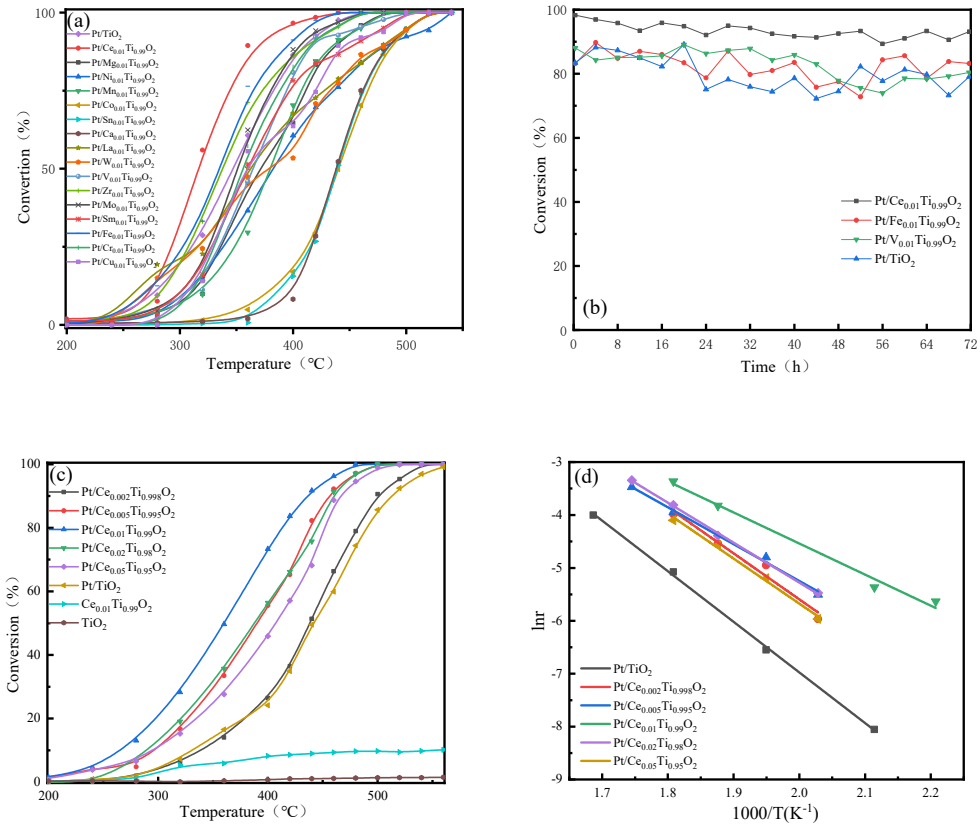

Figure 1. (**a**) Catalytic activity and (**b**) durability at 420 °C of part of M-Pt/TiO_2 catalysts. Reaction conditions: [C_2H_6] = 1000 ppm, [O_2] = 4 vol%, [H_2O] = 5%, [SO_2] = 100 ppm, balance N_2, total flow rate = 200 mL/min, and GHSV = 60,000 h^{-1}. (**c**) Catalytic activity of Pt/$Ce_xTi_{1-x}O_2$ catalysts. Reaction conditions: [C_2H_6] = 1000 ppm, [O_2] = 4 vol%, balance N_2, total flow rate = 200 mL/min, and GHSV = 60,000 h^{-1}. (**d**) Arrhenius plots of Pt/$Ce_xTi_{1-x}O_2$ catalysts.

2.1.2. Catalytic Performance towards SO_2 and H_2O Resistance

Figure 2a shows the activity evaluation curve of the Pt/$Ce_xTi_{1-x}O_2$ (x = 0.002, 0.005, 0.01, 0.02, and 0.05) catalysts under conditions of SO_2 and H_2O. Through the activity evaluation data, it was found that the catalyst still showed good activity when doped with 1% Ce, and the decreasing order of catalytic activity at 90% ethane conversion was as follows: Pt/$Ce_{0.01}Ti_{0.99}O_2$, Pt/$Ce_{0.005}Ti_{0.995}O_2$, Pt/$Ce_{0.02}Ti_{0.98}O_2$, Pt/$Ce_{0.002}Ti_{0.998}O_2$, and Pt/$Ce_{0.05}Ti_{0.95}O_2$. Therefore, the appropriate doping amount of the Ce element is also a significant factor for obtaining the highest catalytic activity even under conditions of SO_2 and H_2O. Moreover, an unexpected promotion of catalytic activity was observed after the introduction of SO_2 and H_2O, which are generally recognized as poisonous in catalytic oxidation. In order to further reveal the roles of SO_2 and H_2O, the Pt/$Ce_{0.01}Ti_{0.99}O_2$ catalyst with the best activity in Section 2.1.1 was selected for catalytic activity evaluation in different atmospheres (Figure 2b). It was evident that the highest catalytic activity of the catalyst was found in atmosphere C, followed by atmosphere A, atmosphere B, and atmosphere D. Specifically, the introduction of H_2O in the reaction inhibited the reaction, which is consistent with the phenomenon of most VOC catalytic oxidation reactions [16]. Figures S2 and S3 indicate that the water molecules and reactants only constitute competitive adsorption on the surface of the catalyst, and its effect on the reactivity is reversible, which further proves that the catalyst has good water stability. In contrast, SO_2 presented a catalytic impact and thus promoted the catalytic reaction, which can be explained by the fact that catalytic activity can be improved by the interaction between sulfate on the surface and highly oxidized platinum atoms on the edge of platinum particles [17].

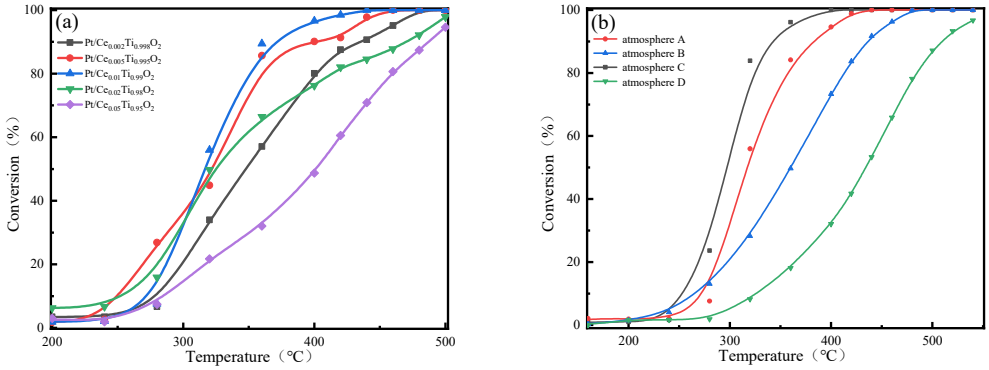

Figure 2. (**a**) Catalytic activity of $Pt/Ce_xTi_{1-x}O_2$ catalysts. Reaction conditions: $[C_2H_6]$ = 1000 ppm, $[O_2]$ = 4 vol%, $[H_2O]$ = 5%, $[SO_2]$ = 100 ppm, balance N_2, total flow rate = 200 mL/min, and GHSV = 60,000 h^{-1}. (**b**) Catalytic activity of $Pt/Ce_{0.01}Ti_{0.99}O_2$ catalysts in different atmospheres. Atmosphere A: 1000 ppm ethane, 4% oxygen, N_2 balance, 100 ppm SO_2, and 5% water. Atmosphere B: 1000 ppm ethane, 4% oxygen, and N_2 balance. Atmosphere C: 1000 ppm ethane, 4% oxygen, N_2 balance, and 100 ppm SO_2. Atmosphere D: 1000 ppm ethane, 4% oxygen, N_2 balance, and 5% water.

2.2. XRD

The XRD characterization results of the $Pt/Ce_xTi_{1-x}O_2$ (x = 0, 0.002, 0.005, 0.01, 0.02, and 0.05) catalysts describing all crystal forms of anatase-TiO_2 are shown in Figure 3a. The diffraction peaks appearing at 25.4°, 37.0°, 37.9°, 38.6°, 48.1°, 54.0°, 55.1°, 62.1°, 68.8°, 75.9°, and 77.4° belong to the (101), (103), (004), (112), (200), (105), (211), (213), (116), (320), and (202) crystal planes, respectively (JCPDS No. 21-1272). No Ce species were found in the XRD spectra of TiO_2 nanoparticles doped with metal elements, which might have been due to deficient doping amounts of Ce ions. In this case, Ti^{4+} cannot be replaced in the lattice position, and it is hard to form a large number of corresponding oxides [18]. At the same time, the diffraction peaks of platinum species were not found either, suggesting high dispersion of Pt [19]. With the increase in the Ce-doping amount, the diffraction peak of TiO_2 gradually weakened, indicating the decrease in crystallinity or particle size of TiO_2. Additionally, from Figure 3b, it can be seen that the main peak of (101) shifted to a smaller angle with the increase in the doping amount, which indicates lattice expansion of TiO_2 [20]. Lattice expansion is mainly due to the fact that the radius of Ce^{4+} (0.092 nm) is much larger than that of Ti^{4+} (0.068 nm), which cannot replace the position of the original titanium atom. Instead, some metal elements enter the lattice and become interstitial atoms, expanding the lattice of TiO_2, leading to large lattice distortion and strain energy. The oxygen atoms on the surface of TiO_2 escape from the lattice to form oxygen defects [21], thus improving the catalytic activity.

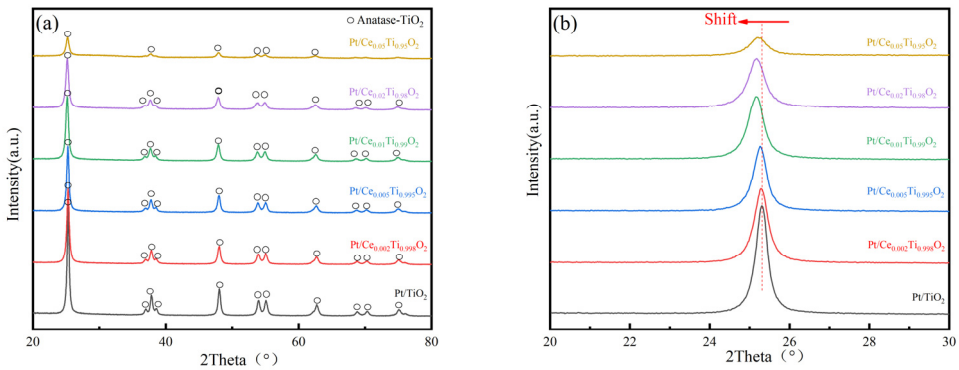

Figure 3. (**a**) XRD patterns and (**b**) partially enlarged detail of XRD patterns of $Pt/Ce_xTi_{1-x}O_2$ catalysts.

Note that with the increase in the Ce-doping amount, the peak position of the $Pt/Ce_{0.01}Ti_{0.99}O_2$ catalyst showed the maximum offset. However, with a further increase in

the doping amount, there was a slight variation in the main peak position of (101), since CeO_2 may be generated in the process of peak intensity weakening but cannot be detected with XRD. In this case, no more Ce ions can exist in the lattice, and the largest number of oxygen vacancies in the $Pt/Ce_{0.01}Ti_{0.99}O_2$ catalyst may be achieved. This phenomenon is further discussed in the following sections.

2.3. Physisorption

Figure 4 shows the N_2 adsorption–desorption isotherms and pore size distribution of the $Pt/Ce_xTi_{1-x}O_2$ (x = 0.002, 0.005, 0.01, 0.02, and 0.05) catalysts. The isotherms of all catalysts belong to the IV-type, and H1-type hysteresis loops between P/P_0 = 0.5 and 0.9 can also be observed, indicating that the five samples had a mesoporous structure. From the shape of the hysteresis loop, it can be determined that the pores had mixed cylindrical and ink-bottle-like features, and that the pore size distribution of the $Pt/Ce_xTi_{1-x}O_2$ catalysts was uniform [22]. The specific surface area, pore volume, and pore size distribution of the catalysts are provided in Table 2. The $Pt/Ce_{0.05}Ti_{0.95}O_2$ catalyst exhibited a certain degree of amorphous structure and a high specific surface area, which is consistent with the XRD results. With the increase in Ce content, the specific surface area and pore volume increased, while the pore size decreased. Due to the difference in the specific surface area of each catalyst, it is necessary to normalize the apparent activity to the specific surface area, that is, the specific activity of the catalyst needs to be compared. As shown in Figure S4, the $Pt/Ce_{0.01}Ti_{0.99}O_2$ catalyst still exhibited the highest specific activity.

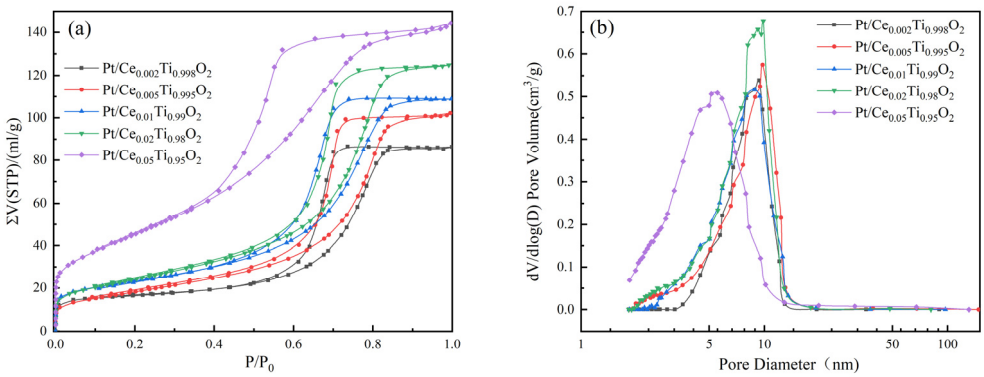

Figure 4. (**a**) Nitrogen adsorption–desorption isotherms and (**b**) pore size distribution curves of $Pt/Ce_xTi_{1-x}O_2$ catalysts.

Table 2. Specific surface areas, O_2-TPD, and XPS results of catalysts.

Catalyst	Physisorption			O_2-TPD			XPS			
	Surface Area (m^2/g)	Pore Volume (cm^3/g)	Average Pore Diameter (nm)	Temperature of α Peak (°C)	Temperature of β Peak (°C)	Aβ/Aα [1]	Ti $2p_{3/2}$ (eV)	$Pt^0/Pt^{2+}+Pt^0$	$O_{latt.}$ conc. [2] (%)	Ce^{3+}/Ce_{total}
Pt/TiO_2	48.40	0.13	10.29	250.10	420.68	1.33	459.58	-	0.86	-
$Pt/Ce_{0.02}Ti_{0.98}O_2$	53.47	0.14	7.66	228.62	404.06	1.52	458.19	0.33	0.81	0.38
$Pt/Ce_{0.05}Ti_{0.95}O_2$	66.78	0.17	7.20	232.49	383.23	2.42	458.42	0.41	0.60	0.55
$Pt/Ce_{0.01}Ti_{0.99}O_2$	81.14	0.19	6.87	227.18	382.87	2.90	458.28	0.49	0.88	0.56
$Pt/Ce_{0.02}Ti_{0.98}O_2$	87.70	0.21	6.89	236.10	439.08	2.39	458.28	0.48	0.87	0.43
$Pt/Ce_{0.05}Ti_{0.95}O_2$	168.32	0.23	4.48	266.18	439.02	1.55	458.18	0.41	0.77	0.39

[1] Calculated using integral areas of O_2-TPD peaks. [2] $O_{latt.}$ concentrations were estimated using ($O_{latt.}/O_{latt.}$ + $O_{ads.}$) × 100% from XPS.

2.4. SEM

Figure 5 presents the morphology and element distribution of $Pt/Ce_xTi_{1-x}O_2$ (x = 0, 0.002, 0.005, 0.01, 0.02, and 0.05). It can be seen that the six catalysts were characterized

by disordered agglomeration of irregular composite metal oxide nanoparticles. With the increase in Ce content, the phenomenon of catalyst particle agglomeration tended to be more obvious. EDS showed that the distribution of Pt and Ce in the $Pt/Ce_xTi_{1-x}O_2$ catalysts was uniform, which is consistent with the results of XRD. Good dispersion can improve the contact between the Pt active species and the reaction gas molecules and promote the catalytic oxidation reaction [23].

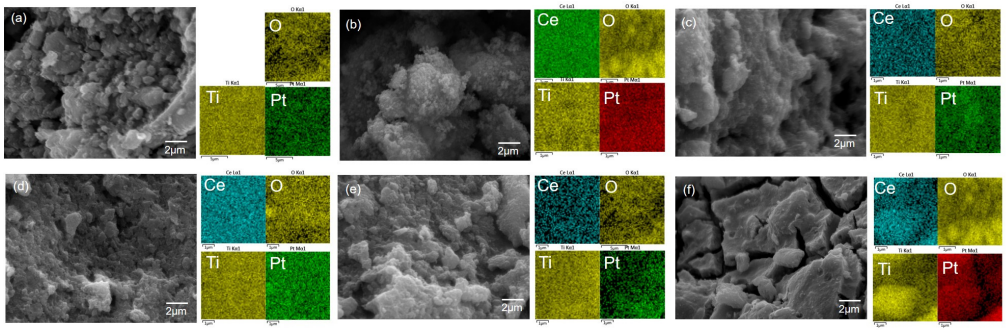

Figure 5. SEM images of $Pt/Ce_xTi_{1-x}O_2$ catalysts: (**a**) Pt/TiO_2, (**b**) $Pt/Ce_{0.002}Ti_{0.998}O_2$, (**c**) $Pt/Ce_{0.005}Ti_{0.995}O_2$, (**d**) $Pt/Ce_{0.01}Ti_{0.99}O_2$, (**e**) $Pt/Ce_{0.02}Ti_{0.98}O_2$, and (**f**) $Pt/Ce_{0.05}Ti_{0.95}O_2$.

2.5. XPS

Figure 6 shows the XPS spectra of Ti 2p, Pt 4f, O 1s, and Ce 3d of the Pt/TiO_2 and $Pt/Ce_xTi_{1-x}O_2$ (x = 0.002, 0.005, 0.01, 0.02, and 0.05) catalysts, and the quantified data are summarized in Table 2. The XPS spectra of the Ti 2p orbitals of the Pt/TiO_2 and $Pt/Ce_xTi_{1-x}O_2$ catalysts are described in Figure 6a. Peaks corresponding to Ti 2p can be divided into two peaks at the binding energies of 458.2–459.5 eV and 463.9–465.2 eV, both of which represent Ti^{4+}. Compared with the Pt/TiO_2 catalyst, obvious shifts in the Ti $2p_{3/2}$ and Ti $2p_{1/2}$ peaks to the lower binding energy region can be observed in all spectra of the catalysts with the doping of Ce (Table 2), which is attributed to the strong Ce–Ti interaction ($Ce^{4+} + Ti^{3+} \rightarrow Ce^{3+} + Ti^{4+}$) in the $Pt/Ce_xTi_{1-x}O_2$ catalysts [24].

Figure 6b shows the Pt 4f orbital XPS spectra of the Pt/TiO_2 and $Pt/Ce_xTi_{1-x}O_2$ catalysts. Pt/TiO_2 was observed to have two obvious characteristic peaks at the binding energies of 72.3 eV and 75.7 eV, which were attributed to the $4f_{7/2}$ and $4f_{5/2}$ orbitals of Pt^{2+}, respectively [25]. However, from the XPS spectra of $Pt/Ce_xTi_{1-x}O_2$ doped with a certain amount of Ce, it was found that the position of the peak evidently shifted to a lower binding energy. After peak fitting, spectra could be divided into two groups, where one represented the characteristic peak with binding energies of 70.5–70.9 eV and 74.0–74.3 eV, belonging to metal element Pt^0 [26], and the other represented the $4f_{7/2}$ and $4f_{5/2}$ orbital peaks of Pt^{2+} at 72.3 eV and 75.7 eV. The results show that Pt existed in the forms of an oxidation state and metal in the catalysts. Generally, after Ce-doping, Pt ions preferentially locate at the Pt/Ce interface; thus, CeO_2 tends to intensively interreact with Pt single atoms compared with Pt nanoclusters or nanoparticles [24]. The initial C-H bond was broken at the site, forming C_2H_5 and a hydroxyl group on the surface, and this is where the reaction took place [27]. Under this condition, more fresh structural defects at the interface between Pt and support were generated, and $Pt/Ce_xTi_{1-x}O_2$ catalysts doped with Ce showed better activity than Pt/TiO_2. The highest relative content of Pt^0 in the $Pt/Ce_{0.01}Ti_{0.99}O_2$ catalyst was 49% (Table 2), which was higher than that of $Pt/Ce_{0.02}Ti_{0.98}O_2$ (48%), $Pt/Ce_{0.005}Ti_{0.995}O_2$ (41%), $Pt/Ce_{0.05}Ti_{0.95}O_2$ (41%), and $Pt/Ce_{0.002}Ti_{0.998}O_2$ (33%). Moreover, the low valence of Pt was beneficial to the catalytic oxidation reaction [28]. Therefore, the $Pt/Ce_{0.01}Ti_{0.99}O_2$ catalyst showed better catalytic activity.

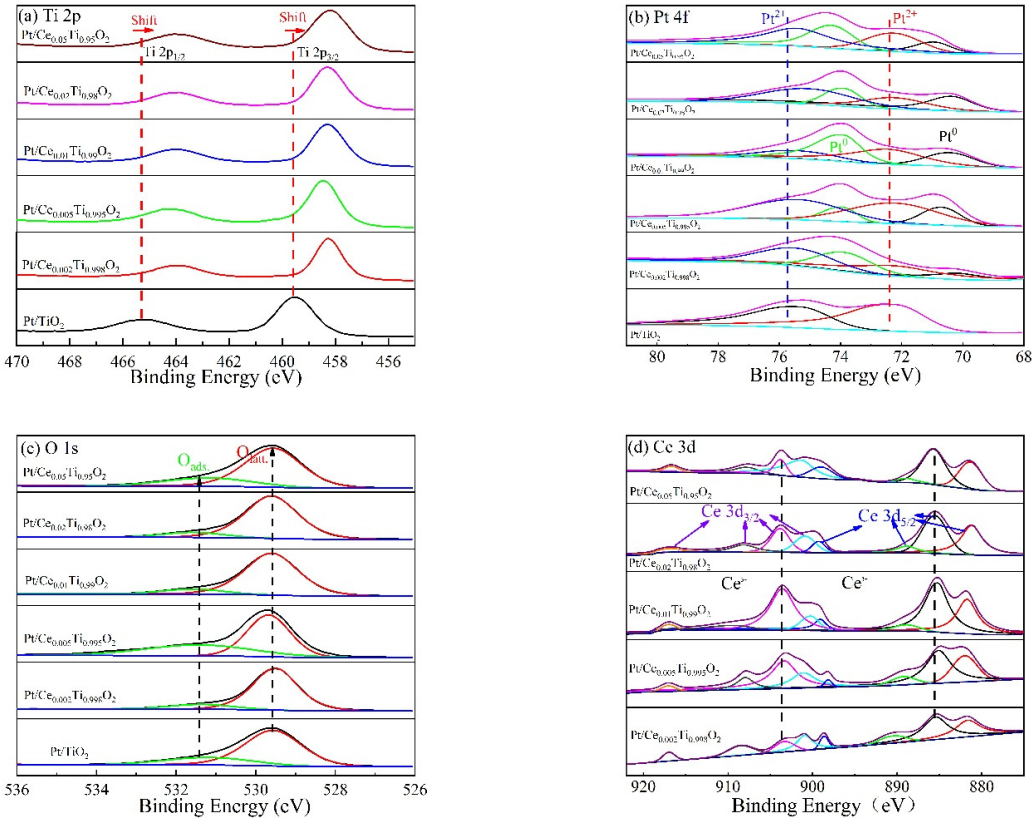

Figure 6. XPS spectra of $Pt/Ce_xTi_{1-x}O_2$ catalysts: (**a**) Ti 2p, (**b**) Pt 4f, (**c**) O 1s, and (**d**) Ce 3d.

Figure 6c shows the O 1s orbital spectra of the Pt/TiO_2 and $Pt/Ce_xTi_{1-x}O_2$ catalysts. All the spectra could be fitted to the peaks of surface-adsorbed oxygen ($O_{ads.}$) and surface lattice oxygen ($O_{latt.}$), where the peak of $O_{ads.}$ was at 531.7 eV and that of $O_{latt.}$ was at 529.8 eV [29]. The $O_{latt.}$ concentration (shown in Table 2) decreased in the following order: $Pt/Ce_{0.01}Ti_{0.99}O_2$ (88%) > $Pt/Ce_{0.02}Ti_{0.98}O_2$ (87%) > Pt/TiO_2 (86%) > $Pt/Ce_{0.002}Ti_{0.998}O_2$ (81%) > $Pt/Ce_{0.05}Ti_{0.95}O_2$ (77%) > $Pt/Ce_{0.005}Ti_{0.995}O_2$ (60%). Specifically, $Pt/Ce_{0.01}Ti_{0.99}O_2$ and $Pt/Ce_{0.02}Ti_{0.98}O_2$ showed the highest $O_{latt.}$ relative contents, 88% and 87%, respectively. Catalysts doped with 1% and 2% Ce exhibited relatively better activity, since the oxygen species involved in the reaction were mainly O_{latt} during the deep oxidation reaction process of ethane.

Figure 6d shows the Ce 3d orbital spectra of the prepared $Pt/Ce_xTi_{1-x}O_2$ catalysts. They could be fitted into eight parts, where 881.6 eV, 885.3 eV, 890.6 eV, and 898.6 eV belong to the Ce $3d_{5/2}$ orbital and 901.1 eV, 903.2 eV, 908.4 eV, and 917.0 eV belong to the Ce $3d_{3/2}$ orbital [30]. Among them, BE = 885.3 and 903.2 eV belong to Ce^{3+}, while the other peaks belong to Ce^{4+}. It is generally believed that higher concentrations of Ce^{3+} species are associated with more oxygen vacancies on the catalyst surface [31]. By quantitatively analyzing the relative content of Ce^{3+}, the calculated amount of Ce^{3+}/Ce_{total} was sorted as follows: $Pt/Ce_{0.01}Ti_{0.99}O_2$ (56%) > $Pt/Ce_{0.005}Ti_{0.995}O_2$ (55%) > $Pt/Ce_{0.02}Ti_{0.98}O_2$ (43%) > $Pt/Ce_{0.002}Ti_{0.998}O_2$ (39%) > $Pt/Ce_{0.05}Ti_{0.95}O_2$ (38%) (see Table 2). $Pt/Ce_{0.01}Ti_{0.99}O_2$ contained the highest Ce^{3+} relative content, 56, and accordingly, the most oxygen vacancies. The more oxygen vacancies form, the higher the catalytic activity of the catalyst is. Therefore, the 1% Ce-doped $Pt/Ce_xTi_{1-x}O_2$ catalyst had relatively good activity, which is consistent with the conclusion of XRD. This was followed by 0.5% and 2% doping amounts of catalyst activity and then 5% and 0.2% doping amounts of catalyst activity.

2.6. O_2-TPD Analysis

The performance of ethane oxidation is closely related to the oxygen storage capacity of the catalyst. The O_2-TPD results of the $Pt/Ce_xTi_{1-x}O_2$ (x = 0, 0.002, 0.005, 0.01, 0.02, and 0.05) catalysts are studied in this section and are shown in Figure 7a. All catalysts showed three desorption peaks near 230, 400, and 700 °C, which can be expressed as α, β, and γ, i.e., the desorption of surface-adsorbed oxygen species, the desorption of surface lattice oxygen, and the thermal decomposition of the catalyst, respectively. Since the Ce element has a good oxygen storage performance, it can be seen intuitively from the figure that as the doping amount of Ce increased, the O_2 desorption peak area of the α and β peaks gradually increased, indicating that the oxygen storage capacity of the catalyst was enhanced. The quantitative data obtained from the peak fitting of the curve are shown in Table 2. It has been reported that α and β oxygen species can participate in catalytic oxidation through a surface mechanism and an MVK mechanism [32], respectively. The desorption temperature of the α peak and the β peak of $Pt/Ce_{0.01}Ti_{0.99}O_2$ was lower than that of other catalysts, which directly reflects that the surface-adsorbed oxygen species and surface lattice oxygen species were more active than those of other catalysts. During the catalytic oxidation of ethane, oxygen absorbed on the surface and stored in $Pt/Ce_{0.01}Ti_{0.99}O_2$ in the lattice state was first activated, which resulted in a better catalytic performance than that of other catalysts. However, lattice-state oxygen became predominant with the promotion of oxidation and participated in the whole process. Generally, the ratio between two desorption peak areas (A_β/A_α) represents the relative amount of active lattice oxygen on the catalyst surface [33], and a more relative amount of active lattice oxygen facilitates the catalytic oxidation reaction. As shown in Table 2, after calculation, A_β/A_α could be sorted as $Pt/Ce_{0.01}Ti_{0.99}O_2$ (2.90) > $Pt/Ce_{0.005}Ti_{0.995}O_2$ (2.40) > $Pt/Ce_{0.02}Ti_{0.98}O_2$ (2.39) > $Pt/Ce_{0.05}Ti_{0.95}O_2$ (1.55) > $Pt/Ce_{0.002}Ti_{0.998}O_2$ (1.52). The obtained pattern is consistent with the T_{90} results of the catalyst evaluation (Table 1), proving that surface lattice oxygen is positively correlated with the deep catalytic oxidation of ethane. Consequently, among these catalysts, $Pt/Ce_{0.01}Ti_{0.99}O_2$, with the largest A_β/A_α and abundant active surface lattice oxygen, was proven to have the best catalytic oxidation performance.

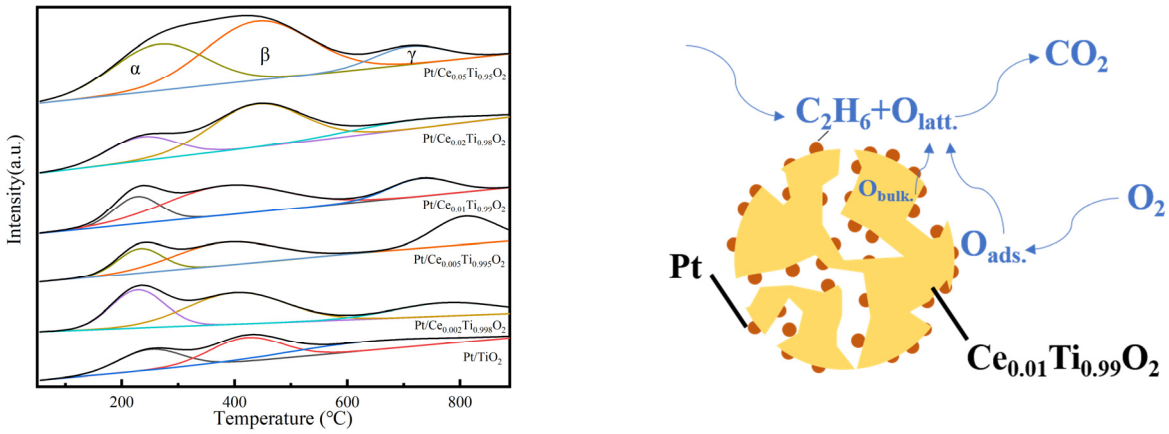

(**a**) (**b**)

Figure 7. (**a**) O_2-TPD profiles of $Pt/Ce_xTi_{1-x}O_2$ (x = 0, 0.002, 0.005, 0.01, 0.02, and 0.05) catalysts. (**b**) Reaction mechanism section of the $Pt/Ce_{0.01}Ti_{0.99}O_2$ catalyst.

Interestingly, the $Pt/Ce_{0.01}Ti_{0.99}O_2$ catalyst exhibited the maximum surface lattice oxygen concentration and oxygen vacancies. Unlike CO catalytic oxidation, ethane catalytic combustion is an interfacial reaction, and the main oxygen species involved in the reaction are lattice oxygen species. In the catalytic oxidation reaction, after lattice oxygen is consumed, the generated oxygen vacancies are supplemented by surface oxygen, and finally

the surface oxygen vacancies are supplemented by gas-phase oxygen. In addition, surface lattice oxygen is supplemented by the rapid movement of bulk lattice oxygen through oxygen vacancies to achieve oxygen migration and participate in interfacial reactions, while bulk lattice oxygen cannot directly participate in the reaction (see Figure 7b) [34,35].

2.7. H_2-TPR Analysis

The H_2-TPR results of the $Pt/Ce_xTi_{1-x}O_2$ (x = 0, 0.002, 0.005, 0.01, 0.02, and 0.05) catalysts and the corresponding supports, $Ce_{0.01}Ti_{0.99}O_2$ and TiO_2, are studied in this section and are shown in Figure 8. There was a strong reduction peak between 310 and 330 °C for all samples. After doping with Ce, the reduction peak of the carrier TiO_2 sample moved to a lower temperature and continued shifting to further lower regions with the loading of the Pt noble metal, which reflects the interaction between the active Pt component and the Ce- and TiO_2-doped elements [36]. The reduction temperature of all $Pt/Ce_xTi_{1-x}O_2$ reduction peaks was higher than that of Pt/TiO_2. This can be explained by the formation of the $Ce_2Ti_2O_7$ solid solution, which can form weak Ce-O and Ti-O bonds, further improve the mobility of lattice oxygen, and promote the catalytic oxidation reaction, according to past studies [37]. Therefore, the promotion of catalytic activity obtained by doping the Ce element was again proven based on this result. Among the $Pt/Ce_xTi_{1-x}O_2$ (x = 0.002, 0.005, 0.01, 0.02, and 0.05) catalyst systems, $Pt/Ce_{0.01}Ti_{0.99}O_2$ had the lowest reduction temperature (320 °C) and the largest reduction peak area, indicating that it had the best redox ability and exhibited the highest activity.

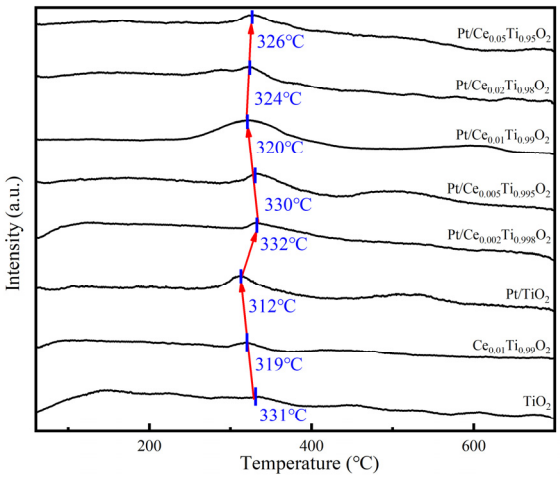

Figure 8. H_2-TPR profiles of $Pt/Ce_xTi_{1-x}O_2$ (x = 0, 0.002, 0.005, 0.01, 0.02, and 0.05) catalysts and $Ce_{0.01}Ti_{0.99}O_2$ and TiO_2 carriers.

2.8. NH_3-TPD Analysis

The surface acidity of the catalyst is related to the catalytic activity. The NH_3-TPD results of the $Pt/Ce_xTi_{1-x}O_2$ (x = 0.002, 0.005, 0.01, 0.02, and 0.05) catalysts are studied in this section and are shown in Figure 9. The obtained curves were fitted into several peaks, and all catalysts showed two desorption peaks. The desorption peaks between 100 and 200 °C and between 200 and 350 °C represent weak acid and medium acid [38], respectively, and are denoted as peaks A and B, respectively (see Figure 9). The data obtained after further quantification are shown in Table 3. It was found that the relative acid content of the catalysts significantly decreased with the increase in the doping amount. After calculation, the relative content of medium acid was sorted as follows: $Pt/Ce_{0.01}Ti_{0.99}O_2$ (80.41%) > $Pt/Ce_{0.005}Ti_{0.995}O_2$ (80.03%) > $Pt/Ce_{0.02}Ti_{0.98}O_2$ (76.78%) > $Pt/Ce_{0.002}Ti_{0.998}O_2$ (72.13%) > $Pt/Ce_{0.05}Ti_{0.95}O_2$ (75.55%). $Pt/Ce_{0.01}Ti_{0.99}O_2$ had the highest relative number of medium acid sites and exhibited the best activity. According to relevant literature reports, medium acids play a decisive role in VOC catalytic oxidation [39,40], and the broad peak centered at medium acid sites could also be assigned to NH_3 weakly absorbed on Brønsted acid sites.

The increase of Brønsted acid sites will improve the redox capacity of the catalyst, thereby improving the catalytic activity [41].

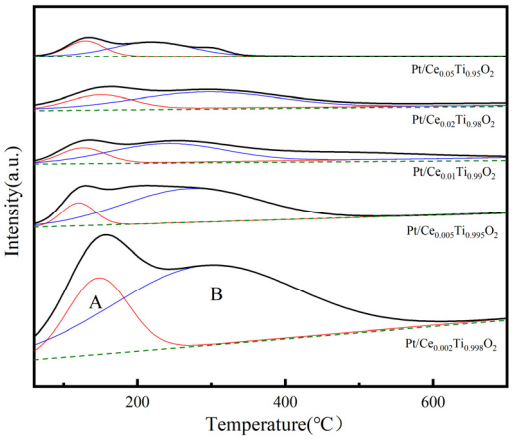

Figure 9. NH_3-TPD profiles of $Pt/Ce_xTi_{1-x}O_2$ (x = 0.002, 0.005, 0.01, 0.02, and 0.05) catalysts. (A: weak acid and B: medium acid).

Table 3. NH_3-TPD results of $Pt/Ce_xTi_{1-x}O_2$ (x = 0.002, 0.005, 0.01, 0.02, and 0.05) catalysts.

Catalyst	Weak	Medium	Total [1]	Weak (%)	Medium (%)
$Pt/Ce_{0.02}Ti_{0.98}O_2$	2.28	7.18	9.46	24.45	75.55
$Pt/Ce_{0.05}Ti_{0.95}O_2$	0.88	3.52	4.40	19.97	80.03
$Pt/Ce_{0.01}Ti_{0.99}O_2$	0.33	1.34	1.67	19.59	80.41
$Pt/Ce_{0.02}Ti_{0.98}O_2$	0.42	1.39	1.81	23.22	76.78
$Pt/Ce_{0.05}Ti_{0.95}O_2$	0.25	0.65	0.90	27.86	72.13

[1] The total acidity amount of the $Pt/Ce_{0.05}Ti_{0.95}O_2$ sample was assumed to be 0.90.

3. Materials and Methods

3.1. Preparation of Catalysts

$Ti(SO_4)_2$, $Ce(NO_3)_2{\cdot}6H_2O$, and $Pt(NO_3)_2$ solutions (18.06 wt%) were purchased from Shanghai Aladdin Biochemical Technology Co., Ltd., Shanghai, China. $NH_3{\cdot}H_2O$ (25 wt%) and ($HO(CH_2CH_2O)_nH$) were purchased from Sinopharm Chemical Reagent Co., Ltd, Shanghai, China. Deionized water was made in our laboratory. The above reagents were analytically pure and directly used in the experiments.

Certain amounts of $Ti(SO_4)_2$ and $Ce(NO_3)_2{\cdot}6H_2O$ (Ce:Ti (molar ratio) = 0/0.2/0.5/1/2/5:100/99.8/99.5/99/98/95) were weighed, dissolved in water, and dropped into $NH_3{\cdot}H_2O$ for precipitation; then, after 24 h of hydrothermal reaction, they were filtered and washed to obtain uncalcined carriers. $Pt(NO_3)_2$ with a mass fraction of 1 wt% was loaded on the above carrier using the excessive impregnation method, dried at 100 °C for 12 h, and calcined at 450 °C for 5 h. $Pt/Ce_xTi_{1-x}O_2$ catalysts were obtained.

3.2. Characterization

The physicochemical properties of the catalysts were characterized by means of X-ray diffraction (XRD; RigakuMiniFlex600; Rigaku, Tokyo, Japan). N_2 adsorption–desorption measurements were conducted using Micromeritics ASAP 2460 equipment. The morphology and chemical composition of the samples were characterized using field-emission scanning electron microscopy (FESEM; Tescan MIRA3LMH, TESCAN, California, USA). The X-ray photo-electron spectrometer (XPS) used was a Thermo Scientific K-Alpha+ (ThermoFisher, Thermo Fisher Scientific, Massachusetts, USA) photoelectron spectrometer. The binding energies of all elements were corrected using the standard C 1s line at 284.6 eV. A Micro-Meritics AutoChem II-2920 chemical adsorption instrument (Micromeritics, Georgia, USA) was implemented to perform H_2 temperature-programmed reduction (H_2-TPR),

O_2 temperature-programmed desorption (O_2-TPD), and NH_3 temperature-programmed desorption (NH_3-TPD). A total of 0.03 g of catalyst was loaded into a quartz tube for H_2-TPR. For 60 min, the catalyst was pretreated in Ar at 300 °C. After cooling to room temperature, a 10 vol% H_2/Ar gas mixture was introduced into the reactor vessel at a flow rate of 20 mL/min. Finally, the catalyst was warmed to 700 °C at a rate of 10 °C/min. In the sample chamber, 0.05 g of precursor was loaded for O_2-TPD. The pretreatment was analogous to that for H_2-TPR. Mixed gas of 4 vol% O_2/Ar at a flow rate of 20 mL/min was added after cooling to 40 °C for 30 min for adsorption. The catalyst was then heated to 800 °C at a ramping rate of 10 °C/min after being flushed with Ar for 60 min. Finally, 0.03 g of catalyst for NH_3-TPD was placed into the sample chamber. The catalyst underwent 1 h of pretreatment in He at 300 °C. Mixed gas of 10% NH_3/He was injected after reaching a temperature of 40 °C at a flow rate of 20 mL/min for 30 min to achieve adsorption. The catalyst was then heated to 700 °C at a ramping rate of 10 °C/min after being flushed with He for 60 min. During the reaction rates test, it is necessary to control the ethane conversion rate below 15% by adjusting the airspeed at the specific temperature. Reaction conditions were: $[C_2H_6]$ = 1000 ppm, $[O_2]$ = 4 vol%, $[H_2O]$ = 5%, $[SO_2]$ = 100 ppm, and balance N_2.

3.3. Catalytic Evaluation

In a fixed-bed continuous-flow quartz reactor (10 mm i.d.) at temperatures between 100 and 560 °C, 0.2 g of catalyst was used for the activity experiments (40–60 mesh). Reaction conditions were: $[C_2H_6]$ = 1000 ppm, $[O_2]$ = 4 vol%, $[H_2O]$ = 5% (when used), $[SO_2]$ = 100 ppm (when used), balance N_2, total flow rate = 200 mL/min, and GHSV = 60,000 h^{-1}. A GC-4000A (EWAI) gas chromatograph (GC) equipped with an FID detector was used to measure the ethane concentration at the inlet (C^{in}) and outflow (C^{out}) of the reactor in real time. Ethane conversion (η) was determined as follows:

$$\eta = \frac{C^{in} - C^{out}}{C^{in}} \times 100\%$$

4. Conclusions

In this work, $Pt/Ce_xTi_{1-x}O_2$ (x = 0, 0.002, 0.005, 0.01, 0.02, and 0.05) catalysts were successfully prepared by means of an in situ metal-doping co-precipitation method. The catalytic activity of the catalysts in different reaction atmospheres was screened. The doping of Ce with a larger atomic radius caused the lattice expansion of TiO_2, resulting in large lattice distortion and oxygen vacancies, which improved the catalytic activity. Excess or insufficient amounts of doping reduced the catalyst activity. Through H_2-TPR, XPS, and other characterization methods, it was found that with Ce-doping, the catalytic oxidation performance was improved as a result of the interaction among the Ce-doping element, TiO_2, and Pt, which led to abundant active lattice oxygen on the catalyst surface and rapid supplementation caused by abundant oxygen vacancies. This study provides practical value for the use of doping strategies to modify catalysts and enhance the ability of the catalytic oxidation of VOCs.

Supplementary Materials: The following supporting information can be downloaded at: https://www.mdpi.com/article/10.3390/catal13030626/s1, Figure S1: Catalytic activity of $Pt/Ce_{0.01}Ti_{0.99}O_2$ catalysts in the low-temperature range. Reaction conditions: $[C_2H_6]$ = 1000 ppm, $[O_2]$ = 4 vol%, balance N_2, total flow rate = 200 mL/min, and GHSV = 60,000 h^{-1}. Figure S2: Durability test at 540 °C of $Pt/Ce_{0.01}Ti_{0.99}O_2$ catalyst under moisture condition. Reaction conditions: $[C_2H_6]$ = 1000 ppm, $[O_2]$ = 4 vol%, $[H_2O]$ = 5%, balance N_2, total flow rate = 200 mL/min, and GHSV = 60,000 h^{-1}. Figure S3: Durability test at 370 °C of $Pt/Ce_{0.01}Ti_{0.99}O_2$ catalyst under moisture condition. Reaction conditions: $[C_2H_6]$ = 1000 ppm, $[O_2]$ = 4 vol%, $[H_2O]$ = 5%, balance N_2, total flow rate = 200 mL/min, and GHSV = 60,000 h^{-1}. Figure S4: Specific reaction rates of $Pt/Ce_{0.01}Ti_{0.99}O_2$ catalysts at 280 °C.

Author Contributions: Conceptualization, D.W. and X.R.; methodology, D.W.; validation, D.W., X.R. and J.Y.; formal analysis, D.W.; investigation, D.W., X.L. and C.H.; resources, J.H.; data curation, J.H.; writing—original draft preparation, D.W.; writing—review and editing, Q.M., J.H. and J.Y.; visualization, D.W.; supervision, J.Y. and J.H.; project administration, J.Y. and J.H.; funding acquisition, X.R. and J.H. All authors have read and agreed to the published version of the manuscript.

Funding: This research was funded by The Central Government Guides Local Science and Technology Development Fund Project (YDZJSX2021B006), the Basic Research Program of Shanxi Province (No. 20210302124450), and the Program of Shanxi Zhejiang University New Materials and Chemical Research Institute (2021SX-TD007).

Data Availability Statement: Not applicable.

Conflicts of Interest: The authors declare no conflict of interest.

References

1. Hien, T.T.; Huy, D.H.; Dominutti, P.A.; Thien Chi, N.D.; Hopkins, J.R.; Shaw, M.; Forster, G.; Mills, G.; Le, H.A.; Oram, D. Comprehensive volatile organic compound measurements and their implications for ground-level ozone formation in the two main urban areas of Vietnam. *Atmos. Environ.* **2022**, *269*, 118872. [CrossRef]
2. Zulkifli, M.F.H.; Hawari, N.S.S.L.; Latif, M.T.; Hamid, H.H.A.; Mohtar, A.A.A.; Idris, W.M.R.W.; Mustaffa, N.I.H.; Juneng, L. Volatile organic compounds and their contribution to ground-level ozone formation in a tropical urban environment. *Chemosphere* **2022**, *302*, 134852. [CrossRef] [PubMed]
3. He, C.; Cheng, J.; Zhang, X.; Douthwaite, M.; Pattisson, S.; Hao, Z. Recent Advances in the Catalytic Oxidation of Volatile Organic Compounds: A Review Based on Pollutant Sorts and Sources. *Chem. Rev.* **2019**, *119*, 4471–4568. [CrossRef] [PubMed]
4. Suciu, G.; Pasat, A.; Balaceanu, C.M.; Balanescu, M.; Nadrag, C. Assessment of the impact of volatile organic compounds (VOC) on human health in sensitive areas. *Proc. SPIE* **2018**, *10977*, 109770S.
5. Kamal, M.S.; Razzak, S.A.; Hossain, M.M. Catalytic oxidation of volatile organic compounds (VOCs)—A review. *Atmos. Environ.* **2016**, *140*, 117–134. [CrossRef]
6. Jian, Y.; Yu, T.; Jiang, Z.; Yu, Y.; Douthwaite, M.; Liu, J.; Albilali, R.; He, C. In-Depth Understanding of the Morphology Effect of α-Fe_2O_3 on Catalytic Ethane Destruction. *ACS Appl. Mater. Interfaces* **2019**, *11*, 11369–11383. [CrossRef]
7. Guo, M.; Li, K.; Zhang, H.; Min, X.; Liang, J.; Hu, X.; Guo, W.; Jia, J.; Sun, T. Promotional removal of oxygenated VOC over manganese-based multi oxides from spent lithium-ions manganate batteries: Modification with Fe, Bi and Ce dopants. *Sci. Total Environ.* **2020**, *740*, 139951. [CrossRef]
8. Yu, X.; Deng, J.; Liu, Y.; Jing, L.; Gao, R.; Hou, Z.; Zhang, Z.; Dai, H. Enhanced Water Resistance and Catalytic Performance of Ru/TiO_2 by Regulating Brønsted Acid and Oxygen Vacancy for the Oxidative Removal of 1,2-Dichloroethane and Toluene. *Environ. Sci. Technol.* **2022**, *56*, 11739–11749. [CrossRef]
9. Yoo, M.; Yu, Y.-S.; Ha, H.; Lee, S.; Choi, J.-S.; Oh, S.; Kang, E.; Choi, H.; An, H.; Lee, K.-S.; et al. A tailored oxide interface creates dense Pt single-atom catalysts with high catalytic activity. *Energy Environ. Sci.* **2020**, *13*, 1231–1239. [CrossRef]
10. Ye, J.; Cheng, B.; Yu, J.; Ho, W.; Wageh, S.; Al-Ghamdi, A.A. Hierarchical Co_3O_4-NiO hollow dodecahedron-supported Pt for room-temperature catalytic formaldehyde decomposition. *Chem. Eng. J.* **2022**, *430*, 132715. [CrossRef]
11. Peng, H.; Ying, J.; Zhang, J.; Zhang, X.; Peng, C.; Rao, C.; Liu, W.; Zhang, N.; Wang, X. La-doped Pt/TiO_2 as an efficient catalyst for room temperature oxidation of low concentration HCHO. *Chin. J. Catal.* **2017**, *38*, 39–47. [CrossRef]
12. Chen, Q.-Y.; Li, N.; Luo, M.-F.; Lu, J.-Q. Catalytic oxidation of dichloromethane over Pt/CeO_2–Al_2O_3 catalysts. *Appl. Catal. B Environ.* **2012**, *127*, 159–166. [CrossRef]
13. Shi, Y.; Wang, J.; Zhou, R. Pt-support interaction and nanoparticle size effect in Pt/CeO_2–TiO_2 catalysts for low temperature VOCs removal. *Chemosphere* **2021**, *265*, 129127. [CrossRef] [PubMed]
14. Huang, K.; Lin, L.; Yang, K.; Dai, W.; Chen, X.; Fu, X. Promotion effect of ultraviolet light on NO+CO reaction over Pt/TiO_2 and Pt/CeO_2–TiO_2 catalysts. *Appl. Catal. B Environ.* **2015**, *179*, 395–406. [CrossRef]
15. Feng, Y.; Ma, P.; Wang, Z.; Shi, Y.; Wang, Z.; Peng, Y.; Jing, L.; Liu, Y.; Yu, X.; Wang, X.; et al. Synergistic Effect of Reactive Oxygen Species in Photothermocatalytic Removal of VOCs from Cooking Oil Fumes over $Pt/CeO_2/TiO_2$. *Environ. Sci. Technol.* **2022**, *56*, 17341–17351. [CrossRef]
16. Ma, X.; Shen, J.; Pu, W.; Sun, H.; Pang, Q.; Guo, J.; Zhou, T.; Cao, H. Water-resistant Fe–Ca–O_x/TiO_2 catalysts for low temperature 1,2-dichlorobenzene oxidation. *Appl. Catal. A Gen.* **2013**, *466*, 68–76. [CrossRef]
17. Corro, G.; Fierro, J.L.G.; Odilon, V.C. An XPS evidence of Pt^{4+} present on sulfated Pt/Al_2O_3 and its effect on propane combustion. *Catal. Commun.* **2003**, *4*, 371–376. [CrossRef]
18. Fan, X.; Liu, D.; Sun, X.; Yu, X.; Li, D.; Yang, Y.; Liu, H.; Diao, J.; Xie, Z.; Kong, L.; et al. Mn-doping induced changes in Pt dispersion and PtxMny alloying extent on Pt/Mn-DMSN catalyst with enhanced propane dehydrogenation stability. *J. Catal.* **2020**, *389*, 450–460. [CrossRef]

19. Hu, D.; Fan, W.; Liu, Z.; Li, L. Three-Dimensionally Hierarchical Pt/C Nanocomposite with Ultra-High Dispersion of Pt Nanoparticles as a Highly Efficient Catalyst for Chemoselective Cinnamaldehyde Hydrogenation. *Chem. Cat. Chem.* **2018**, *10*, 779–788. [CrossRef]
20. Zhao, Y.; Zhao, Y.; Shi, R.; Wang, B.; Waterhouse, G.I.N.; Wu, L.-Z.; Tung, C.-H.; Zhang, T. Tuning Oxygen Vacancies in Ultrathin TiO_2 Nanosheets to Boost Photocatalytic Nitrogen Fixation up to 700 nm. *Adv. Mater.* **2019**, *31*, 1806482. [CrossRef]
21. Fang, J.; Bi, X.; Si, D.; Jiang, Z.; Huang, W. Spectroscopic studies of interfacial structures of CeO_2–TiO_2 mixed oxides. *Appl. Surf. Sci.* **2007**, *253*, 8952–8961. [CrossRef]
22. Thommes, M.; Kaneko, K.; Neimark, A.V.; Olivier, J.P.; Rodriguez-Reinoso, F.; Rouquerol, J.; Sing, K.S.W. Physisorption of gases, with special reference to the evaluation of surface area and pore size distribution (IUPAC Technical Report). *Pure Appl. Chem.* **2015**, *87*, 1051–1069. [CrossRef]
23. Stefa, S.; Lykaki, M.; Fragkoulis, D.; Binas, V.; Pandis, P.K.; Stathopoulos, V.N.; Konsolakis, M. Effect of the Preparation Method on the Physicochemical Properties and the CO Oxidation Performance of Nanostructured CeO_2/TiO_2 Oxides. *Processes* **2020**, *8*, 847. [CrossRef]
24. Shi, Y.; Guo, X.; Wang, Y.; Kong, F.; Zhou, R. New insight into the design of highly dispersed Pt supported CeO_2–TiO_2 catalysts with superior activity for VOCs low-temperature removal. *Green Energy Environ.* **2022**, *in press*. [CrossRef]
25. Svintsitskiy, D.A.; Kibis, L.S.; Stadnichenko, A.I.; Koscheev, S.V.; Zaikovskii, V.I.; Boronin, A.I. Highly Oxidized Platinum Nanoparticles Prepared through Radio-Frequency Sputtering: Thermal Stability and Reaction Probability towards CO. *Chemphyschem* **2015**, *16*, 3318–3324. [CrossRef]
26. Fu, J.; Zhang, X.; Li, H.; Chen, B.; Ye, S.; Zhang, N.; Yu, Z.; Zheng, J.; Chen, B. Enhancing electronic metal support interaction (EMSI) over Pt/TiO_2 for efficient catalytic wet air oxidation of phenol in wastewater. *J. Hazard. Mater.* **2022**, *426*, 128088. [CrossRef]
27. Descorme, C.; Jacobs, P.W.; Somorjai, G.A. Catalytic Combustion of Ethane over Palladium Foil in the 300–450 °C Range: Kinetics and Surface Composition Studies. *J. Catal.* **1998**, *178*, 668–678. [CrossRef]
28. Kim, G.J.; Lee, S.M.; Chang Hong, S.; Kim, S.S. Active oxygen species adsorbed on the catalyst surface and its effect on formaldehyde oxidation over Pt/TiO2 catalysts at room temperature; role of the Pt valence state on this reaction? *RSC Adv.* **2018**, *8*, 3626–3636. [CrossRef]
29. Liu, H.; Sun, C.; Fan, Z.; Jia, X.; Sun, J.; Gao, F.; Tang, C.; Dong, L. Doping effect of Sm on the TiO_2/CeSmOx catalyst in the NH_3-SCR reaction: Structure–activity relationship, reaction mechanism and SO_2 tolerance. *Catal. Sci. Technol.* **2019**, *9*, 3554–3567. [CrossRef]
30. Hou, J.; Hu, J.; Bao, W.; Yao, J.; Wu, D.; Wang, J.; Wang, B.; Zeng, Z.; Cui, X.; Su, S.; et al. Effects of Ti modified CeCu mixed oxides on the catalytic performance and SO2 resistance towards benzene combustion. *Catal. Commun.* **2023**, *174*, 106596. [CrossRef]
31. Zhang, T.; Qiu, W.; Zhu, H.; Ding, X.; Wu, R.; He, H. Promotion Effect of the Keggin Structure on the Sulfur and Water Resistance of Pt/CeTi Catalysts for CO Oxidation. *Catalysts* **2022**, *12*, 4. [CrossRef]
32. Fang, Y.; Li, L.; Yang, J.; Hoang, S.; Wang, L.; Xu, J.; Yang, W.; Pan, C.; Zhu, Y.; Deng, H.; et al. Engineering the Nucleophilic Active Oxygen Species in CuTiOx for Efficient Low-Temperature Propene Combustion. *Environ. Sci. Technol.* **2020**, *54*, 15476–15488. [CrossRef] [PubMed]
33. Yao, J.; Wu, D.; Yan, X.; Wang, B.; Hu, J.; Bao, W.; Chang, L.; Wang, J. Highly catalytic-performance for benzene oxidation: Effect of oxygen species on OMS-2 by Co doping. *Fuel* **2021**, *305*, 121538. [CrossRef]
34. Dong, C.; Zhou, Y.; Ta, N.; Liu, W.; Li, M.; Shen, W. Shape impact of nanostructured ceria on the dispersion of Pd species. *Chin. J. Catal.* **2021**, *42*, 2234–2241. [CrossRef]
35. Gholizadeh, A.; Malekzadeh, A.; Ghiasi, M. Structural and magnetic features of $La_{0.7}Sr_{0.3}Mn_{1-x}Co_xO_3$ nano-catalysts for ethane combustion and CO oxidation. *Ceram. Int.* **2016**, *42*, 5707–5717. [CrossRef]
36. Kwon, H.C.; Park, Y.; Park, J.Y.; Ryoo, R.; Shin, H.; Choi, M. Catalytic Interplay of Ga, Pt, and Ce on the Alumina Surface Enabling High Activity, Selectivity, and Stability in Propane Dehydrogenation. *ACS Catal.* **2021**, *11*, 10767–10777. [CrossRef]
37. Ruan, C.; Huang, Z.-Q.; Lin, J.; Li, L.; Liu, X.; Tian, M.; Huang, C.; Chang, C.-R.; Li, J.; Wang, X. Synergy of the catalytic activation on Ni and the CeO_2–$TiO_2/Ce_2Ti_2O_7$ stoichiometric redox cycle for dramatically enhanced solar fuel production. *Energy Environ. Sci.* **2019**, *12*, 767–779. [CrossRef]
38. Oh, D.-k.; Lee, Y.-J.; Lee, K.-Y.; Park, J.-S. Nitrogen Monoxide and Soot Oxidation in Diesel Emissions with Platinum–Tungsten/Titanium Dioxide Catalysts: Tungsten Loading Effect. *Catalysts* **2020**, *10*, 1283. [CrossRef]
39. Shi, D.; Fu, G.; Omran, A.; Haw, K.-G.; Zhu, L.; Ding, R.; Lang, Q.; Wang, S.; Fang, Q.; Qiu, S.; et al. Acidic properties of Al-rich ZSM-5 crystallized in strongly acidic fluoride medium. *Microporous Mesoporous Mater.* **2022**, 112332, *in press*. [CrossRef]
40. Lv, L.; Wang, S.; Ding, Y.; Zhang, L.; Gao, Y.; Wang, S. Mechanistic insights into the contribution of Lewis acidity to brominated VOCs combustion over titanium oxide supported Ru catalyst. *Chemosphere* **2021**, *263*, 128112. [CrossRef]
41. Jiang, Y.; Wang, X.; Lai, C.; Shi, W.; Liang, G.; Bao, C.; Ma, S. Effect of Ca Doping on the Selective Catalytic Reduction of NO with NH_3 over Ce–Ti Oxide Catalyst. *Catal. Lett.* **2018**, *148*, 2911–2917. [CrossRef]